Journal for ImmunoTherapy of Cancer

Runx3-overexpression cooperates with ex vivo AKT inhibition to generate receptor-engineered T cells with better persistence, tumor-residency, and antitumor ability

Jianghui Tang,[1,2,3] Jianpeng Sheng,[1,2,3,4] Qi Zhang,[1,2,3] Yongtao Ji,[1,2,3] Xun Wang,[1,2,3] Junlei Zhang,[1,2,3] Jiangchao Wu,[1,2,3] Jinyuan Song,[1,2,3] Xueli Bai ,[1,2,3,4] Tingbo Liang [1,2,3,4]

To cite: Tang J, Sheng J, Zhang Q, *et al*. Runx3-overexpression cooperates with ex vivo AKT inhibition to generate receptor-engineered T cells with better persistence, tumor-residency, and antitumor ability. *Journal for ImmunoTherapy of Cancer* 2023;**11**:e006119. doi:10.1136/jitc-2022-006119

► Additional supplemental material is published online only. To view, please visit the journal online (http://dx.doi.org/10.1136/jitc-2022-006119).

JT, JS and QZ contributed equally.

Accepted 08 February 2023

Check for updates

© Author(s) (or their employer(s)) 2023. Re-use permitted under CC BY-NC. No commercial re-use. See rights and permissions. Published by BMJ.

For numbered affiliations see end of article.

Correspondence to
Professor Tingbo Liang; liangtingbo@zju.edu.cn

ABSTRACT

Background Solid tumors pose unique roadblocks to treatment with chimeric antigen receptor (CAR) T cells, including limited T-cell persistence, inefficient tumor infiltration, and an immunosuppressive tumor microenvironment. To date, attempts to overcome these roadblocks have been unsatisfactory. Herein, we reported a strategy of combining *Runx3* (encoding RUNX family transcription factor 3)-overexpression with ex vivo protein kinase B (AKT) inhibition to generate CAR-T cells with both central memory and tissue-resident memory characteristics to overcome these roadblocks.

Methods We generated second-generation murine CAR-T cells expressing a CAR against human carbonic anhydrase 9 together with *Runx3*-overexpression and expanded them in the presence of AKTi-1/2, a selective and reversible inhibitor of AKT1/AKT2. We explored the influence of AKT inhibition (AKTi), *Runx3*-overexpression, and their combination on CAR-T cell phenotypes using flow cytometry, transcriptome profiling, and mass cytometry. The persistence, tumor-infiltration, and antitumor efficacy of CAR-T cells were evaluated in subcutaneous pancreatic ductal adenocarcinoma (PDAC) tumor models.

Results AKTi generated a CD62L+central memory-like CAR-T cell population with enhanced persistence, but promotable cytotoxic potential. *Runx*3-overexpression cooperated with AKTi to generate CAR-T cells with both central memory and tissue-resident memory characteristics. *Runx3*-overexpression enhanced the potential of CD4+CAR T cells and cooperated with AKTi to inhibit the terminal differentiation of CD8+CAR T cells induced by tonic signaling. While AKTi promoted CAR-T cell central memory phenotype with prominently enhanced expansion ability, *Runx3*-overexpression promoted the CAR-T cell tissue-resident memory phenotype and further enhanced persistence, effector function, and tumor-residency. These novel AKTi-generated *Runx3*-overexpressing CAR-T cells exhibited robust antitumor activity and responded well to programmed cell death 1 blockade in subcutaneous PDAC tumor models.

Conclusions *Runx3*-overexpression cooperated with ex vivo AKTi to generate CAR-T cells with both tissue-resident and central memory characteristics, which equipped CAR-T cells with better persistence, cytotoxic potential, and tumor-residency ability to overcome roadblocks in the treatment of solid tumors.

WHAT IS ALREADY KNOWN ON THIS TOPIC

⇒ Protein kinase B (AKT) inhibition generates CD62L+central memory-like chimeric antigen receptor (CAR)-T cell populations and maintains T-cell persistence. The transcription factor RUNX family transcription factor 3 (RUNX3) promotes tissue resident memory T-cell development, which function as both effector and memory T cells, and additionally express residence gene signatures. However, we lack satisfactory strategies to generate CAR-T cells with both tissue-resident and central-memory characteristics in the field of adoptive cell therapy.

WHAT THIS STUDY ADDS

⇒ *Runx3*-overexpression combined with ex vivo AKT inhibition (AKTi) generated CAR-T cells with central memory and tissue-resident memory characteristics. The AKTi-generated *Runx3*-overexpressing CAR-T cells showed better persistence, cytotoxic potential, tumor residency ability, and antitumor efficacy against solid tumors.

HOW THIS STUDY MIGHT AFFECT RESEARCH, PRACTICE OR POLICY

⇒ The strategy of combining *Runx3*-overexpression with ex vivo AKTi has good potential for clinical application. Moreover, CAR-T therapy could be improved by exploiting the advantages, while ameliorating the disadvantages, of different T-cell phenotypes.

BACKGROUND

Chimeric antigen receptor (CAR) T cells have shown remarkable efficacy in cancer immunotherapy,[1] particularly to treat blood cancers. However, the therapeutic application

of CAR-T cells against solid tumors is challenging.[2] Compared with liquid tumors, solid tumors pose unique roadblocks to CAR-T cell treatment,[2 3] including limited T-cell persistence,[4] inefficient tumor infiltration,[5 6] and an immunosuppressive tumor microenvironment.[7 8] Even when solid tumors express targetable antigens, the antitumor efficacy of CAR-T cells would be unsatisfactory unless all the three roadblocks were overcome.

The adoptive transfer of T cells with less-differentiated phenotypes is critical for antitumor efficacy and patient outcomes, because of their increased expansion, persistence, and ability to differentiate into effector progeny.[49] Attempts to maintain T-cell persistence and stemness have had some success, for example, the use of other homeostatic cytokines instead of interleukin (IL)-2,[10 11] pharmacological inhibition of the phosphatidylinositol-4,5-bisphosphate 3-kinase (PI3K)-protein kinase B (AKT) pathway,[12–14] and activation of Wnt signaling.[15] In fact, AKT inhibition (AKTi) by the inhibitor AKTi-1/2 generated a significant CD62L+central memory-like CAR-T cell population.[12 13] Central memory T cells (Tcms), generated by AKTi, express the lymphoid homing molecules CD62L (also known as selectin L (SELL)) and C-C motif chemokine receptor 7 (CCR7) and have enhanced replicative capacity; however, they also express few of the chemokine receptors or adhesion molecules necessary for trafficking to peripheral tissues and have limited effector function.[16] Thus, a strategy to enhance Tcms' cytotoxic potential and their ability to traffic to disease sites, which does not impair their self-renewal ability and persistence, is required.

Tissue-resident memory T cells (Trms) represent a heterogeneous T-cell population that function as both effector and memory T cells, but also express residence gene signatures, unlike effector memory T cells (Tems).[17] This feature allows them to traffic to, reside in, and potentially patrol peripheral tissues.[17] We wanted to equip Tcms with the properties of Trms, to enhance their cytotoxic potential and tumor infiltration. The transcription factor RUNX family transcription factor 3 (RUNX3) can program CD8+T cell residency in non-lymphoid tissues and tumors.[18] *Runx3*-overexpression (RUNX3-OE) enhanced tumor-infiltrating lymphocyte abundance, and the expression of granzyme B and certain core tissue residency genes, while suppressing core circulating gene expression.[18] Thus, *Runx3*-OE might equip T cells with Trm-like properties.

Herein, we combined ex vivo AKTi with *Runx3*-OE to generate CAR-T cells with tissue-resident and central-memory characteristics. AKTi promoted the CAR-T cell Tcm phenotype and enhanced persistence, whereas *Runx3*-OE promoted the CAR-T cell Trm phenotype and further enhanced persistence, effector function, and tumor residency. To the best of our knowledge, this was the first attempt to create CAR-T cells with tissue-resident and central memory characteristics, allowing them to overcome the roadblocks to treating solid tumors more comprehensively.

METHODS

Cell lines and mice

The KPC cell line, derived from spontaneous tumors in a $Kras^{LSL\text{-}G12D}$; $Trp53^{LSL\text{-}R172H}$; Pdx1-Cre mouse model, was maintained in McCoy's 5A (Modified) Medium (Gibco) supplemented with 10% fetal bovine serum (FBS) (Cat#FBS-E500, NEWZERUM). HEK293T cells (ATCC) and Plat-E cells (Cell Biolabs) were maintained in Dulbecco's Modified Eagle's Medium (Gibco) supplemented with 10% FBS. Bxpc-3 cells (ATCC) were maintained in Roswell Park Memorial Institute (RPMI) 1640 medium (Gibco) supplemented with 10% FBS. KPC and Bxpc-3 cells expressing human carbonic anhydrase 9 (hCA9) was constructed by transduction with lentiviruses containing hCA9 and isolating cell clones using limiting dilution. We relied on the suppliers' data for *Mycoplasma* and cell authenticity testing. All mice were purchased from the Model Animal Research Center of Nanjing University (China) and housed in the specific pathogen free facility of the First Affiliated Hospital, Zhejiang University School of Medicine, with approval from the Institutional Animal Care and Use Committee (ID 20191101).

Plasmid construction

The second-generation murine CAR (mCAR) was constructed using the murine CD8α signal peptide, anti-human-CA9 single-chain variable fragment(scFv),[19] the hinge and transmembrane domains of murine CD8α, and the cytoplasmic domains of murine CD28 and CD3ζ. One copy of strep-tag II was added to the N-terminus between the signal peptide and scFv for surface detection.[20] All retroviral plasmids were based on the pMSCV-IRES-GFP II (pMIGII; Cat#52107, Addgene). To achieve overexpression, genes (mCARs or others) were cloned into pMIGII through the EcoRI and BamHI sites to retain the green fluorescent protein (GFP) tag or through the EcoRI and SalI sites to replace the GFP tag. The murine *Runx3* complementary DNA was linked 3' to the mCAR sequences through a sequence encoding a P2A self-cleaving peptide to achieve co-expression. Gene fragments were generated by chemical synthesis. The final plasmids were confirmed by Sanger sequencing.

Murine primary T-cell activation and isolation

Spleen cells from 8-week-old BALB/c mice were collected and activated using anti-CD3ε and anti-CD28 antibodies for 24 hours.[21] Activated T cells were enriched using Percoll gradient centrifugation.[21] Residual B cells were removed using biotin anti-mouse-CD19 antibodies (BioLegend) and Streptavidin Nanobeads (BioLegend).

Retrovirus production, transduction, and T-cell expansion

The retroviral supernatant was produced in Plat-E cells,[22] and concentrated by ultrafiltration using Amicon Ultra-15 (Millipore). Retrovirus transduction of T cells was performed in 6-well plates by spinning infection with polybrene.[21] At 4 hours post-infection, transduced cells were resuspended and transferred to 10-cm plates

for expansion in the presence of AKTi-1/2 (MedChemExpress) or vehicle (dimethyl sulfoxide). T cells were maintained in RPMI 1640 medium supplemented with 10% FBS, 100 IU/mL IL-2 (Novoprotein) and 0.05 mM 2-mercaptoethanol (Gibco).

Adoptive therapy tumor models

KPC-hCA9 cells (1×10^6/50 µL) were injected into the flanks of 7-week-old male nude mice. Tumor-bearing mice were randomly assigned to groups and T cells were adoptively transferred into mice via intravenous injection. Tumors were measured using electronic digital calipers and the tumor volume was calculated in cm^3 (½ × length×width^2). Mice were euthanized when the tumor length >1.5 cm or the tumor volume >1 cm^3. No mice were excluded during the experiment. For each experiment, mice were purchased at the same time and acclimatized in the same environment for at least 1 week before the experiment.

Statistical analysis

Statistical analysis was performed using Prism software (GraphPad, V.9.0). Shapiro-Wilk test was used to confirm the normal distribution of data. Data for all experiments from at least three biological replicates were presented as means±SEM. One-way (column tables) or two-way (grouped tables) analysis of variance was used for multiple comparisons, and p values were adjusted by Tukey method. Student's t-test was used to compare the differences between two groups. Survival curves were generated using Kaplan-Meier estimates and compared using the log-rank test. P value<0.05 was considered statistically significant.

Supplementary detailed methods and antibodies used were available (online supplemental table 1).

RESULTS

AKTi generated a CD62L+central memory-like CAR-T cell population with enhanced persistence but promotable cytotoxic potential

AKTi was used to preserve a CD62L+Tcm like population. We activated mouse spleen cells using anti-CD3 and CD28 antibodies for 48 hours in the presence of 0–4 µM AKTi-1/2 to determine its optimal working concentration. AKTi-1/2 at 1–2 µM significantly inhibited AKT phosphorylation, but had little effect on total AKT levels (figure 1A). Next, we performed mouse T-cell activation, purification, and retroviral transduction of the second-generation mCAR against hCA9 (online supplemental figure S1A), a protein upregulated in human pancreatic ductal adenocarcinoma (PDAC) samples.[23] CAR-T cells were expanded in the presence of vehicle or 1–2 µM AKTi-1/2, which was maintained during the entire experiment (Mode1) or after retroviral transduction (Mode2) (figure 1B). AKTi-1/2 addition did not influence the retroviral transduction efficiency (online supplemental figure S1B). 1 µM AKTi-1/2 was sufficient to preserve the CD62L+Tcm like population (figure 1C,D) and inhibit AKT phosphorylation during CAR-T cell expansion (online supplemental figure S1C). The time point of AKTi-1/2 addition had little effect on the preservation of the Tcm-like population (figure 1D), because the percentage of Tcm-like cells was high and the degree of AKT phosphorylation was low in the initial stage of CAR-T cell expansion (figure 1D, online supplemental figure S1C). Interestingly, 2 µM AKTi-1/2 treatment retained more Tcm-like cells than 1 µM AKTi-1/2, but inhibited CAR-T cell expansion by approximately twofold (online supplemental figure S1D). Thus, in subsequent experiments, CAR-T cells were expanded in the presence of 1 µM AKTi-1/2 after retroviral transduction, representing the optimal concentration. Transcriptome analysis of sorted CD8+CAR T cells identified the top five most enriched genes following AKTi exposure as *Sell*, *Ccr7*, *Klf2* (KLF transcription factor 2), *S1pr1* (sphingosine-1-phosphate receptor 1), and *Tcf7* (transcription factor 7) (figure 1E), which were all associated with T-cell lymphoid homing and persistence.[24] The overexpression of *Sell* (encoding CD62L) was consistent with the protein expression data measured using flow cytometry. The RNA sequencing (RNA-seq) data also showed that AKTi downregulated the expression of genes and Kyoto Encyclopedia of Genes and Genomes (KEGG) pathway members associated with effector function (figure 1E, online supplemental figure S1E). The downregulation of cell cycle pathways supported the result that a high concentration of AKTi-1/2 inhibited CAR-T cell expansion (online supplemental figure S1E). We confirmed that AKTi downregulated granzyme B (GzmB) levels as well as the cytolytic ability of CD8+CAR T cells (figure 1F,G).

We then adoptively transferred 5 million T cells with 50% CAR-T cells via intravenous injection into tumor-bearing nude mice (online supplemental figure S2A,B). The inguinal lymph nodes were larger in the CAR-T+AKTi group compared with those in the CAR-T group (online supplemental figure S2C). Notably, AKTi would not decrease the percentage of CD8+T cells among CD45+ immune cells or CAR-T cells among T cells (online supplemental figure S2D,E). Thus, AKTi promoted CAR-T cell expansion in lymph nodes. Furthermore, AKTi barely affected tumor infiltration: T-cell counts in tumors showed no significant change (online supplemental figure 2F,G). However, AKTi increased the CD8+CAR T count per mm^3 of tumor (online supplemental figure S2H), indicating the enhanced persistence of tumor-infiltrating CAR-T cells. The tumor volume was not significantly smaller when treated using AKTi-generated CAR-T cells compared with using normal CAR-T cells (online supplemental figure S2I). AKTi-generated Tcm-like cells expressed lymphoid homing molecules CD62L and CCR7, and showed enhanced expansion but a weaker effector function; therefore, we hypothesized that equipping Tcm-like cells with Trm-like properties would improve the weakness of AKTi-generated CAR-T cells and enhance their effector function and tumor infiltration.

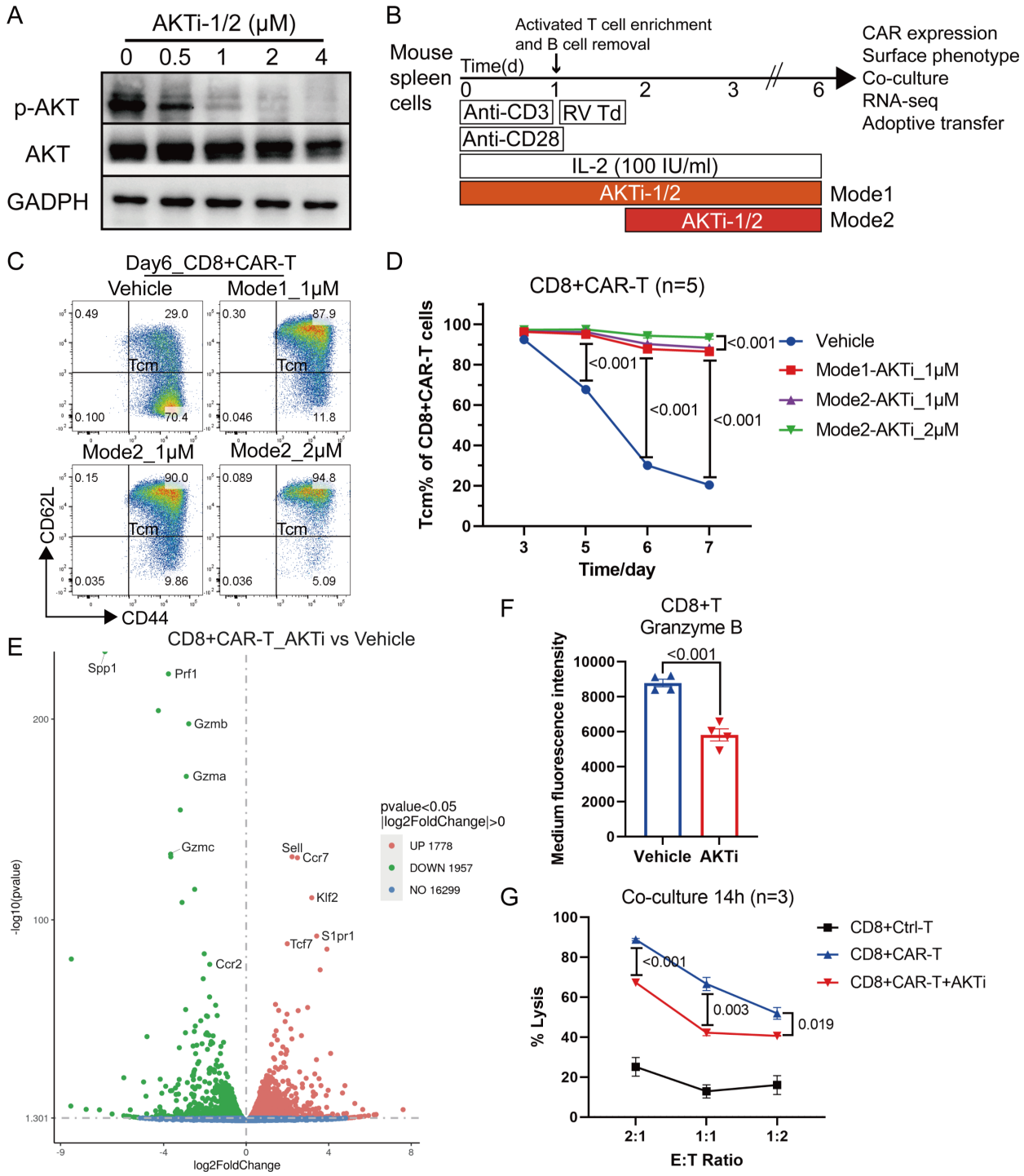

Figure 1 AKTi generated CD62L+central memory-like CAR-T cell population with promotable cytotoxic potential. (A) Western blotting of mouse spleen cells activated by 1 μg/mL anti-mouse CD3 and 0.5 μg/mL anti-mouse CD28 antibodies for 48 hours in the presence of 0–4 μM AKTi-1/2. AKT, Akt (pan); p-AKT, Phospho-Akt (Ser473). (B) Schema for the activation, purification, retroviral transduction (RV Td), and expansion of mouse T cells in the presence of IL-2 (100 IU/mL) and AKTi-1/2 (0–2 μM). AKTi-1/2 was maintained in the entire period (Mode1) or after retroviral transduction (Mode2). (C) Representative flow cytometry plot of CD44+CD62L+Tcm like CD8+CAR T cells. T cells were expanded in 0–2 μM AKTi-1/2 for 6 days. (D) Percentages of Tcm-like cells in CAR-T cells during the course of the culture in 0–2 μM AKTi-1/2. (E) Volcano plot of differentially expressed genes between CD8+CAR T cells expanded in 1 μM AKTi-1/2 (AKTi, Mode2) and vehicle, as quantified by messenger RNA sequencing (n=2 biological replicates each). (F) Medium fluorescence intensity of granzyme B in CD8+T cells measured by flow cytometry. (G) Target-cell lysis activity of CD8+CAR T cells following 14 hours of co-incubation with human carbonic anhydrase 9-overexpressed KPC cells (target cells). A two-way analysis of variance was used for multiple comparisons in panels D and G, and p values were adjusted by Tukey method. An unpaired two-tailed Student's t-test was used between two groups in panel F. P value<0.05 was considered statistically significant. AKT, protein kinase B; AKTi, AKT inhibition; CAR, chimeric antigen receptor; IL, interleukin; RNA-seq, RNA sequencing; Tcm, central memory T cells.

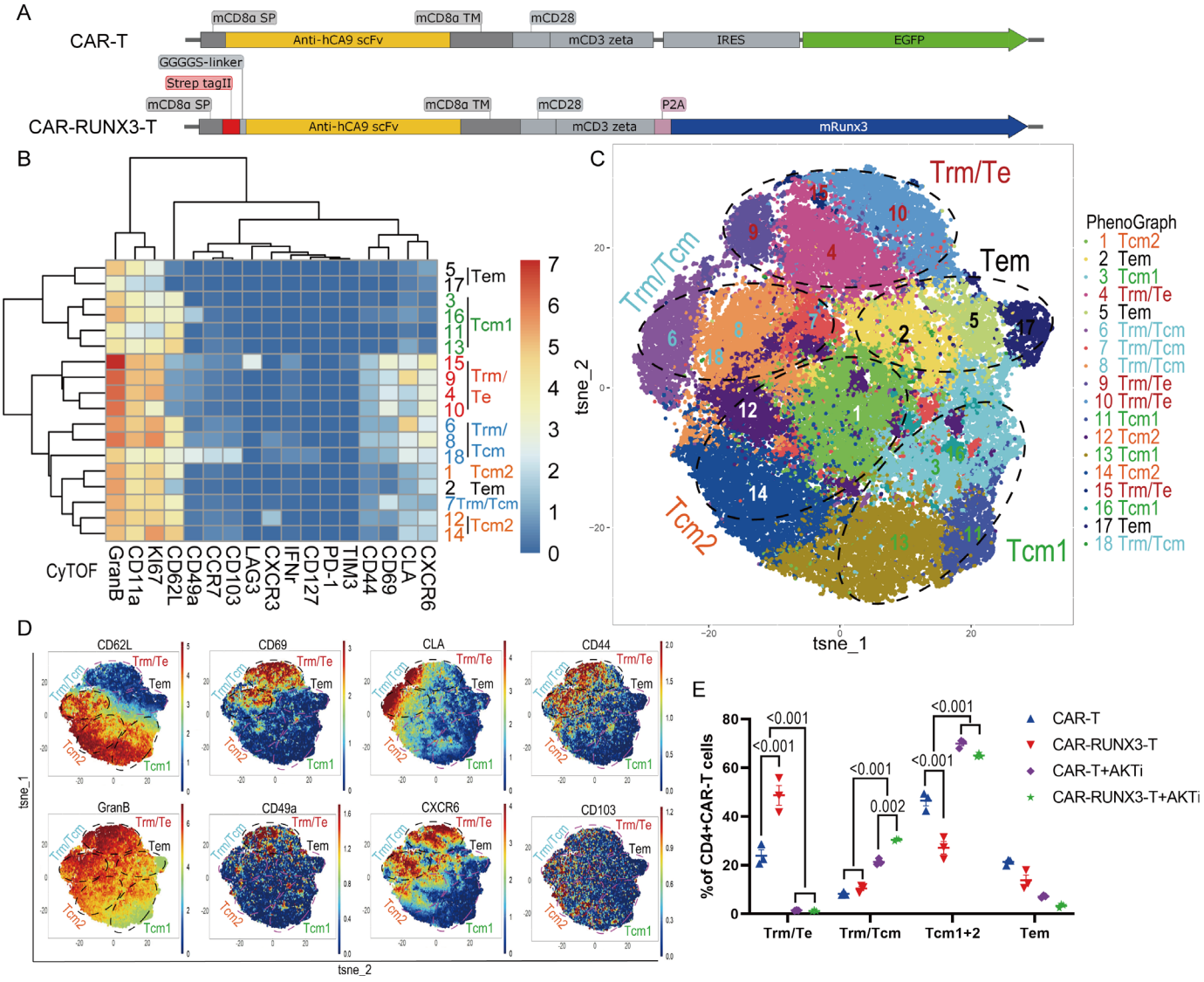

Figure 2 Runx3-overexpression cooperated with AKTi to generate CAR-T cells with both tissue-resident and central memory characteristics in vitro. (A) Schematic diagram of plasmids expressing a second-generation CAR (CAR-T) against human carbonic anhydrase 9 or together with Runx3-overexpression (CAR-RUNX3-T). The CAR and murine Runx3 complementary DNA were separated by a P2A ribosomal skip sequence. The CAR-T plasmid contained a green fluorescent protein tag and the CAR-RUNX3-T plasmid contained a N-terminal Strep-tag II for detecting surface expression. (B) Heatmap of the expression of representative markers associated with Trm and Tcm phenotypes in different CD4+CAR T clusters. T cells were expanded in the presence of 100 IU/mL interleukin-2 and 1 µM AKTi-1/2 or vehicle for 6 days. The expression of markers was quantified by CyTOF and clusters were identified by PhenoGraph method. (C) t-SNE map of CD4+CAR T cells expressing different markers detected by CyTOF. Clusters with similar markers were combined. (D) t-SNE plots of representative markers detected by the CyTOF. (E) Percentages of different T-cell population in CD4+CAR T cells identified by CyTOF. CAR-T, normal CAR-T cells; CAR-RUNX3-T, Runx3-overexpressed CAR-T cells; AKTi, T cells were expended in 1 µM AKTi-1/2. A two-way analysis of variance was used for multiple comparisons in panel E, and p values were adjusted by Tukey method. P value<0.05 was considered statistically significant. AKT, protein kinase B; AKTi, AKT inhibition; CAR, chimeric antigen receptor; CyTOF, cytometry by time of flight; t-SNE, t-distributed stochastic neighbor embedding; RUNX3, RUNX family transcription factor 3; Tcm, central memory T cells; Tems, effector memory T cells; Trms, tissue-resident memory T cells.

Runx3-OE cooperated with AKTi to generate CAR-T cells with both tissue-resident and central-memory characteristics

Transcription factor RUNX3 was reported to program T-cell Trm phenotype[18]; therefore we overexpressed *Runx3* in the AKTi-generated CAR-T cells. To overexpress *Runx3* together with CAR, the CAR and murine RUNX3 were linked by a P2A self-cleaving peptide and an N-terminal strep-tag II was added to detect surface expression (figure 2A).[20] AKTi still preserved the CD62L+Tcm like population in Runx3-OE CAR-T cells (CAR-RUNX3-T) (online supplemental figure S3A), indicating that Runx3-OE did not interfere with AKTi's effect. Then, we explored the effect of AKTi, Runx3-OE and their combination on the CAR-T cell phenotype.

Transcriptomic data showed that both Runx3-OE and AKTi had dynamic effects on CD4+T cells, whereas

Runx3-OE had minimal effects on CD8+T cells (online supplemental figure S3B). Thus, we compared our transcriptomic data of CD4+T cells to the RNA-seq data previously published for Trms[25] using clustering analysis of these core Trm markers (online supplemental figure S3C).[18] Our data showed that the genes downregulated in Trms were suppressed by Runx3-OE, but upregulated by AKTi (online supplemental figure S3D), which supported Runx3-OE promotion of the Trm phenotype and AKTi promotion of the Tcm phenotype. However, the genes upregulated in Trms were intricately influenced by Runx3-OE and AKTi (online supplemental figure S3E). Perhaps the phenotype induced by Runx3-OE and AKTi was a mixture of different phenotypes.

We then measured the expression of Trm-associated markers on CD4+CAR T cells using cytometry by time of flight (CyTOF), which identified 18 clusters using the PhenoGraph method. Based on a heatmap and t-distributed-stochastic neighbor embedding(t-SNE) map, clusters were divided into five groups (figure 2B–D). The Trm/effector-type (Te) group did not express Tcm marker CD62L and showed high levels of GzmB and CD69 as well as other tissue-resident markers, such as CD11a, CLA, CD49a, CD103, and CXCR6 (figure 2B–D).[26] The Trm/Tcm group had high levels of both tissue-resident markers and the Tcm marker, CD62L (figure 2B–D). The Tcm groups had low levels of tissue-resident markers but high levels of CD62L. The Tcm2 group had higher levels of some tissue-resident markers (CXCR6, CLA, and CD44) than Tcm1 (figure 2B–D). AKTi significantly enriched T-cell populations with Tcm characteristics (Tcm and Trm/Tcm groups), while Runx3-OE enriched T-cell populations with Trm characteristics (Trm/Te and Trm/Tcm groups) (figure 2E). The combination of Runx3-OE and AKTi enriched a T-cell population with both Trm and Tcm characteristics (figure 2E). Thus, the CyTOF analysis proved that Runx3-OE cooperated with AKTi to generate CAR-T cells with both tissue-resident and central memory characteristics.

Runx3-OE enhanced the cytotoxic potential of CD4+CAR T cells and cooperated with AKTi to promote CAR-T cell persistence

Next, we evaluated the influence of AKTi and Runx3-OE on CAR-T cells' cytotoxic potential. The transcriptomic data indicated that Runx3-OE upregulated gene expression associated with effector function (figure 3A, online supplemental figure S4A), including *GzmB* and *Nkg7* (natural killer cell granule protein 7). KEGG pathway analysis showed that pathways associated with effector function were also upregulated (online supplemental figure S4B,C). AKTi inhibited the *GzmB* expression and the cytolytic ability of CAR-T cells (figure 3B, online supplemental figure S4D), which was consistent with our previous results (figure 1F–G), while Runx3-OE significantly enhanced the cytolytic ability of AKTi-generated CAR-T cells (figure 3B). AKTi strongly promoted the Tcm-like phenotype; therefore, we withdrew AKTi from the AKTi groups for 24 hours to recover the differentiation of CAR-T cells into other phenotypes. Although there was no significant increase in GzmB in CD8+CAR T cells after Runx3-OE, Runx3-OE did enhance the expression of GzmB in CD4+CAR T cells (figure 3C). Runx3-OE also promoted interferon (IFN)-γ and tumor necrosis factor (TNF)-α expression in CD4+CAR T cells after 6 hours of co-incubation with target cells (figure 3D, online supplemental figure S4E), which supported Runx3-OE-mediated enhancement of the effector function of CD4+CAR T cells. However, IFN-γ and TNF-α expression was downregulated slightly by Runx3-OE in CD8+CAR T cells after 6 hours of co-incubation with target cells (figure 3D, online supplemental figure S4E).

In addition, Runx3-OE enhanced the percentage of CAR-T cells among T cells and the expansion kinetics of sorted CAR-T cells in vitro, especially CD4+T cells (figure 3E–F). Runx3-OE cooperated with AKTi to preserve the Ki67-high population and inhibited the formation of a Ki67-low population on day 7, especially in CD4+T cells (figure 3G–H). These results indicated that Runx3-OE cooperated with AKTi to enhance the expansion ability of CAR-T cells.

In conclusion, Runx3-OE enhanced the cytotoxic potential of CD4+CAR T cells and cooperated with AKTi to promote CAR-T cell persistence by maintaining their proliferation.

Runx3-OE cooperated with AKTi to inhibit the terminal differentiation of CD8+ CAR T cells induced by tonic signaling

We next investigated why Runx3-OE slightly downregulated the cytolytic ability of normal CD8+CAR T cells as well as the expression of IFN-γ and TNF-α after co-incubation with target cells (figure 3B,D). The heatmap of the transcriptomic data showed high baseline levels of effector-related genes in CD8+CAR T cells (figure 4A). Meanwhile, Runx3-OE inhibited the expression of several effector-related genes, including *GzmB*, *Prf1*, and *Ifng* (figure 4A), which was consistent with our previous data showing the downregulated effector function mediated by Runx3-OE (figure 3B,D). We confirmed that the baseline level of IFN-γ was very high in normal CAR-T cells in vitro, but not in control T cells without retroviral transduction (figure 4B), which indicated tonic signaling of CAR-T cells. We then generated new third generation CAR-T cells based on CD28 and 4-1BB (also known as TNF receptor superfamily member 9) co-stimulation domains (online supplemental figure S5A), because 4-1BB co-stimulation could ameliorate tonic signaling-induced T-cell exhaustion.[27] The third generation CAR-T cells exhibited much lower baseline levels of IFN-γ than the second generation CAR-T cells based on CD28 domains (online supplemental figure S5B), further confirming the existence of tonic signaling. Runx3-OE cooperated with AKTi to reduce the baseline expression of IFN-γ (figure 4B, online supplemental figure S5B), PD-1 (programmed cell death 1), and Tim-3 (T-cell immunoglobulin mucin 3) (figure 4C), especially in CD8+T cells. Meanwhile, Runx3-OE, but not the residual P2A peptide, contributed to the downregulation of IFN-γ (online supplemental figure S5C). Runx3-OE also

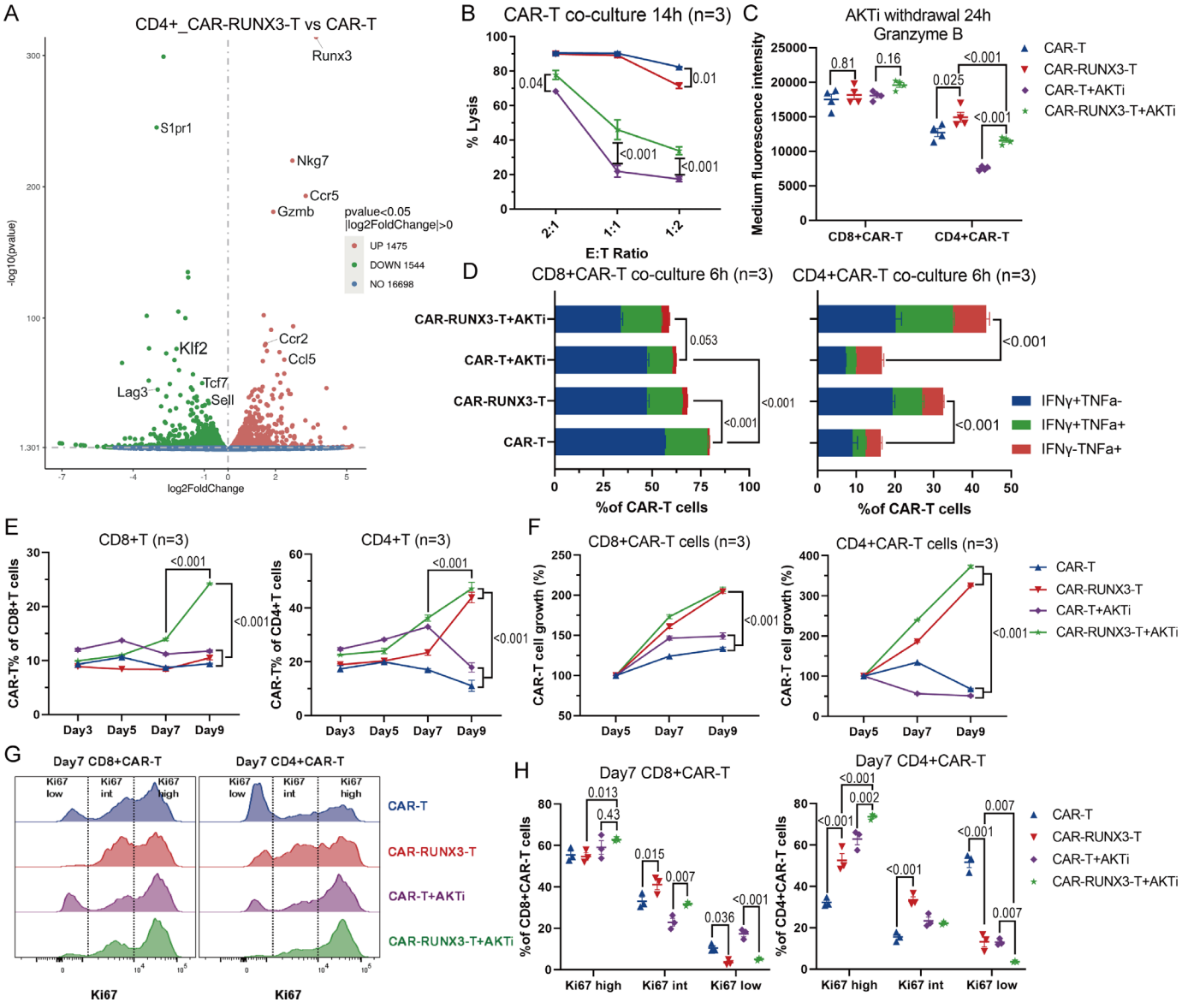

Figure 3 Runx3-overexpression enhanced the cytotoxic potential of CD4+CAR T cells and cooperated with AKTi to promote CAR-T cell persistence. (A) Volcano plot of differentially expressed genes between Runx3-overexpressed CD4+CAR T cells and normal CD4+CAR T cells, as quantified by messenger RNA sequencing (n=2 biological replicates each). (B) Target-cell lysis activity of CAR-T cells following 14 hours of co-incubation with target cells. CAR-T, normal CAR-T cells; CAR-RUNX3-T, Runx3-overexpressed CAR-T cells; AKTi, T cells were expended in 1 µM AKTi-1/2. (C) Medium fluorescence intensity of granzyme B measured by flow cytometry. Before analysis, CAR-T cells of all groups were cultured in the presence of IL-2 but no AKTi for 24 hours. (D) Percentages of IFN-γ and TNF-α expression in CAR-T cells measured by flow cytometry. CAR-T cells of all groups were co-incubated with target cells for 6 hours in the presence of IL-2. (E) Percentages of CAR-T cells in T cells during the course of the culture. (F) Growth curve of sorted CAR-T cells. CAR-T cell growth was defined as the ratio of cell count on a given day to that on day 5. (G) Representative flow cytometry histogram and (H) percentages of Ki67 expression in CAR-T cells after 7 days of expansion. A one or two-way analysis of variance was used for multiple comparisons in panels B, C, D, E, F and H, and p values were adjusted by Tukey method. P value<0.05 was considered statistically significant. AKT, protein kinase B; AKTi, AKT inhibition; CAR, chimeric antigen receptor; IFN, interferon; IL, interleukin; RUNX3, RUNX family transcription factor 3; TNF, tumor necrosis factor.

slowed down the loss of CD62L on CD8+T cells during the late period of expansion (figure 4D,E). The loss of CD62L and the expression of IFN-γ, PD-1, and Tim-3 all indicated the differentiation of CAR-T cells into a terminal phenotype, which was contributed to by tonic signaling. Therefore, Runx3-OE cooperated with AKTi to inhibit CAR-T cell terminal differentiation induced by tonic signaling.

Runx3-OE cooperated with ex vivo AKTi to enhance both the antitumor activity of CAR-T cells and their sensitivity to PD-1 immunotherapy in vivo

Next, the antitumor efficacy of the AKTi-generated CAR-T cells with Runx3-OE was tested in vivo. We sorted GFP+ AKTi-generated CAR-T and strep-tag II+ AKTi-generated CAR-RUNX3-T cells and adoptively transferred them

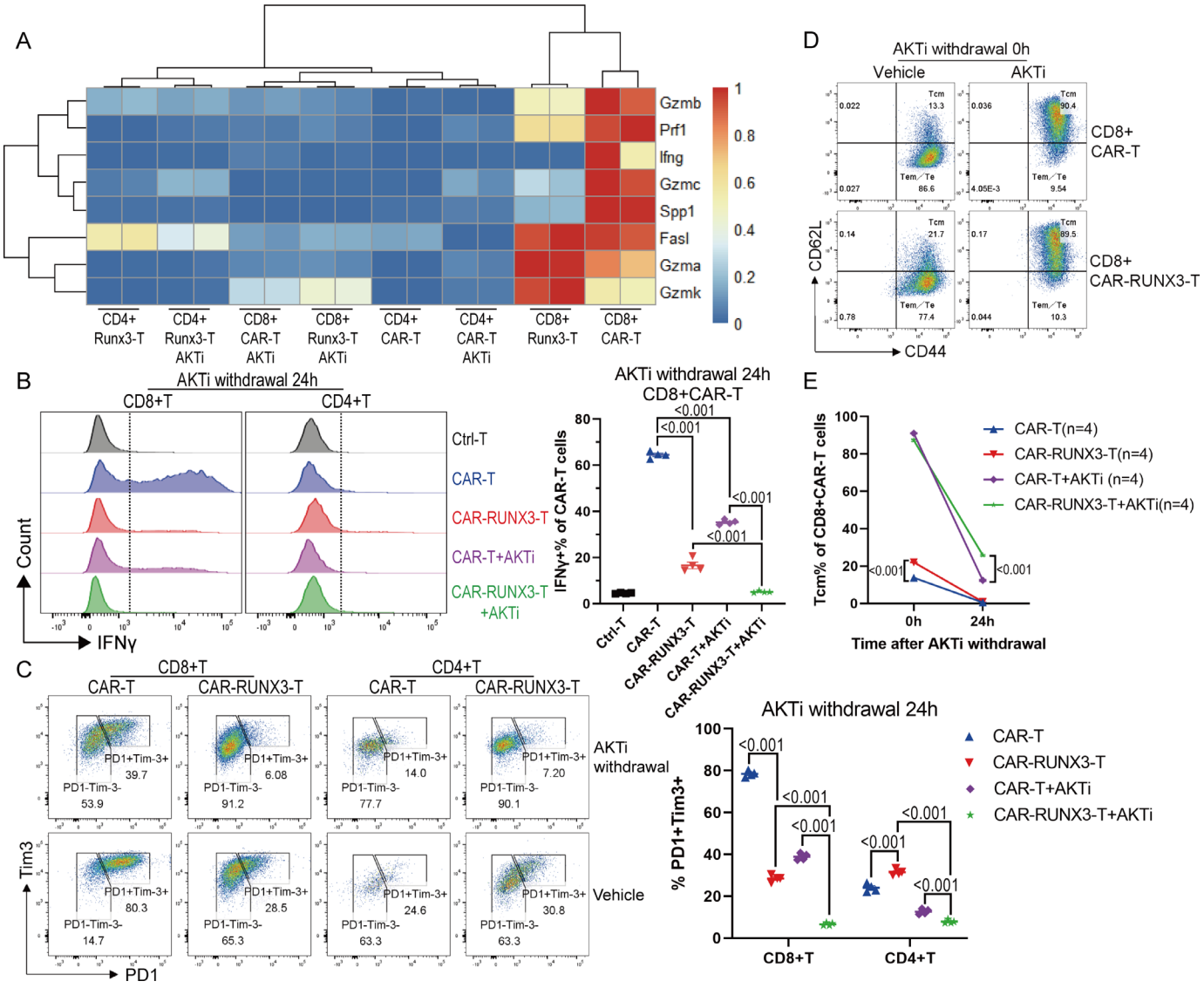

Figure 4 Runx3-overexpression cooperated with AKTi to inhibit terminal differentiation of CD8+CAR T cells induced by tonic signaling. (A) Heatmap of the expression levels of representative genes associated with effector function, as quantified by messenger RNA sequencing. CAR-T, normal CAR-T cells; RUNX3-T, Runx3-overexpressed CAR-T cells; AKTi, T cells were expended in 1 µM AKTi-1/2. (B) Representative flow cytometry histogram and percentages of IFN-γ expression in CAR-T cells. AKTi withdrawal 24 hours, CAR-T cells of all groups were cultured in the presence of interleukin-2 but no AKTi for 24 hours before analysis. Ctrl-T, T cells without retroviral transduction; CAR-RUNX3-T, Runx3-overexpressed CAR-T cells. (C) Representative flow cytometry plot and percentages of PD-1+Tim3+ cells in CAR-T cells. (D–E) Representative flow cytometry plot and percentages of CD44+CD62L+central memory T cells in CD8+CAR T cells after AKTi withdrawal. A one or two-way analysis of variance was used for multiple comparisons in panels B, C and E, and p values were adjusted by Tukey method. P value<0.05 was considered statistically significant. AKT, protein kinase B; AKTi, AKT inhibition; CAR, chimeric antigen receptor; PD-1, programmed cell death 1; RUNX3, RUNX family transcription factor 3; Tim-3, T-cell immunoglobulin mucin 3.

into tumor-bearing mice (online supplemental figure S6A). The number of CAR-T cells was increased to 5 and 10 million, respectively, to enhance the antitumor efficacy and determine the optimized CAR-T cell count for adoptive transfer. The tumor volume was smaller (online supplemental figure S6B), and overall survival (OS) was longer (online supplemental figure S6C) in the CAR-RUNX3-T groups compared with those in the CAR-T groups treated with the same number of CAR-T cells. Notably, treatment with 10 million CAR-RUNX3-T cells eliminated tumors 1 week after adoptive therapy and half of the mice still had no recurrence 90 days later (online supplemental figure S6C,D).

To further verify the contribution of Runx3-OE and AKTi to antitumor efficacy, we generated CAR-RUNX3-T and CAR-T cells in the presence of 1 µM AKTi-1/2 or vehicle. In the previous experiment, 5 million AKTi-generated CAR-RUNX3-T cells exhibited significant antitumor efficacy; therefore, we adoptively transferred 5 million CAR-T cells into tumor-bearing mice

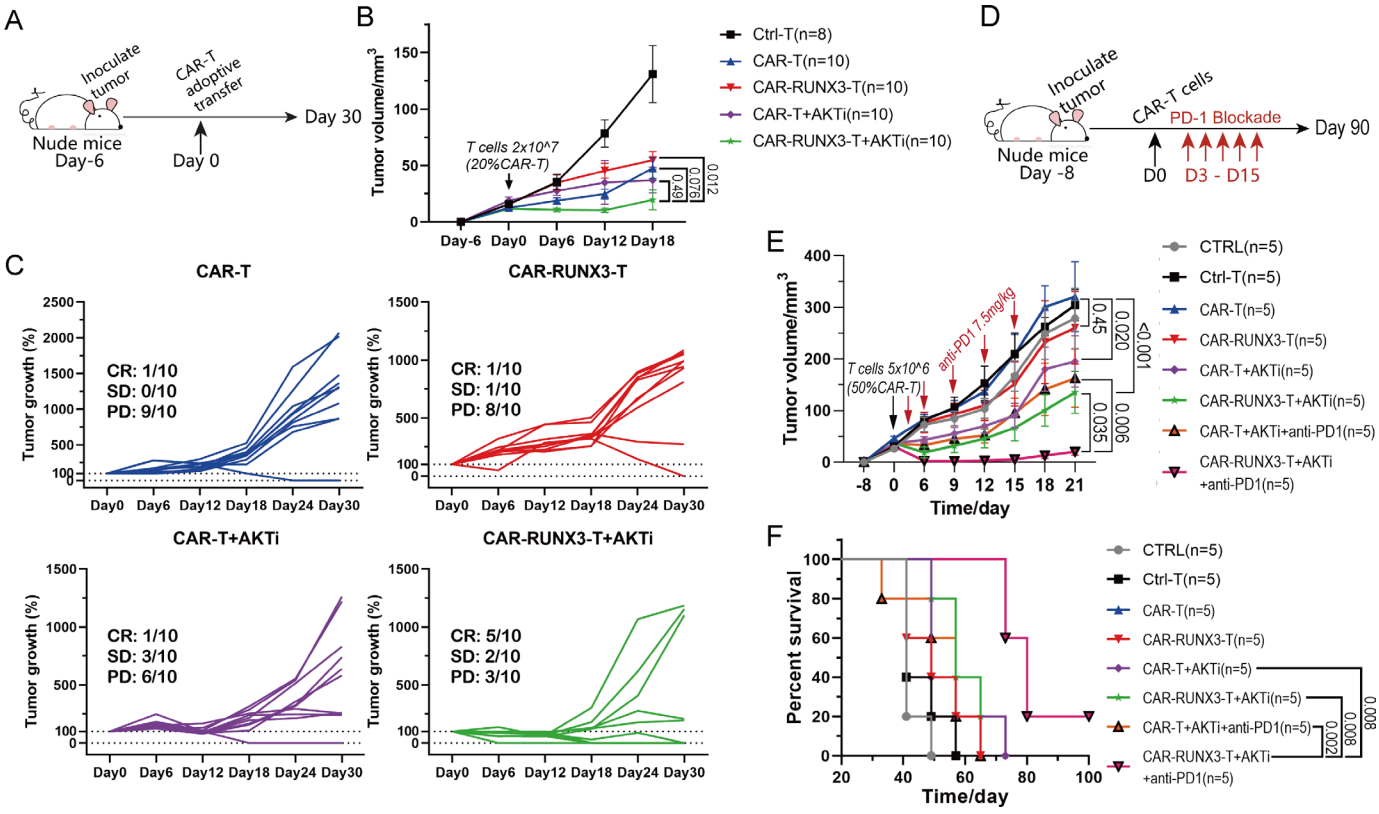

Figure 5 Runx3-overexpression cooperated with ex vivo AKTi to enhance both the antitumor activity of CAR-T cells and the sensitivity to PD-1 immunotherapy in vivo. (A) Schematics of experiment; 2×10^7 T cells with 20% CAR-T cells were adoptively transferred into tumor-bearing nude mice. (B) Tumor progression. Tumor volume was calculated in cubic centimeter (½ × length×width^2). Ctrl-T, T cells without retroviral transduction; CAR-T, normal CAR-T cells; CAR-RUNX3-T, Runx3-overexpressed CAR-T cells; AKTi, T cells were expended in 1 µM AKTi-1/2. (C) Tumor progression. Tumor growth was defined as the ratio of tumor volume on a given day to that on day 0. (D) Schematics of experiment; 5×10^6 T cells with 50% CAR-T cells were adoptively transferred into tumor-bearing nude mice on day 0. PD-1 blockade was performed on day 3–15. (E) Tumor progression. CTRL, no adoptive therapy. (F) Survival curve. P values of survival curve in panel F were calculated by log-rank test analysis. A two-way analysis of variance was used for multiple comparisons in panels B and E, and p values were adjusted by Tukey method. P value<0.05 was considered statistically significant. AKT, protein kinase B; AKTi, AKT inhibition; CAR, chimeric antigen receptor; CR, complete response; PD, progressive disease; PD-1, programmed cell death 1; RUNX3, RUNX family transcription factor 3; SD, stable disease.

(figure 5A). Around day 18, CAR-T therapy suppressed tumor growth in all groups; however, the AKTi-generated CAR-RUNX3-T cells exhibited the best antitumor activity (figure 5B). After day 18, some tumors began to grow rapidly. We divided tumors into three groups according to their growth trend: complete response (CR, tumors disappeared without recurrence), stable disease (SD, tumors existed but grew by no more than 30% every 6 days), and progressive disease (PD, tumors grew by more than 30% every 6 days). The CAR-RUNX3-T+AKTi group showed the highest proportion of CR (5/10) and the least proportion of PD (3/10) among the four groups (figure 5C), indicating the best antitumor activity. Furthermore, AKTi-generated CAR-RUNX3-T cells responded well to PD-1 blockade while AKTi-generated CAR-T cells did not (figure 5D–F). The combination of AKTi-generated CAR-RUNX3-T cells and PD-1 blockade resulted in the smallest tumor volume and longest OS (figure 5D–F). These results confirmed the robust antitumor activity of AKTi-generated CAR-RUNX3-T cells. Thus, Runx3-OE cooperated with AKT inhibition to enhance both the antitumor activity of CAR-T cells and their sensitivity to PD-1 immunotherapy in vivo.

Runx3-OE cooperated with ex vivo AKTi to enrich the T-cell population with both Trm and Tcm characteristics in vivo

Next, we explored the lasting impact of Runx3-OE/AKTi-generated CAR-T cells on the in vivo phenotype. We determined the expression of Trm-associated markers on CD8+CAR T cells in lymph nodes using CyTOF, and 16 clusters were identified using PhenoGraph (figure 6A). Based on the heatmap and the t-SNE map, clusters were divided into four groups (figure 6B,C). The Trm group had high expression of CD69 as well as other tissue resident markers, such as CXCR6 and CLA (figure 6B, online supplemental figure S7A). The Trm/Tcm group had both Trm and Tcm characteristics (expression of Trm markers as well as the Tcm marker CCR7) (figure 6B, online supplemental figure S7A). The Tem groups showed low expression of both Trm marker CD69 and Tcm marker

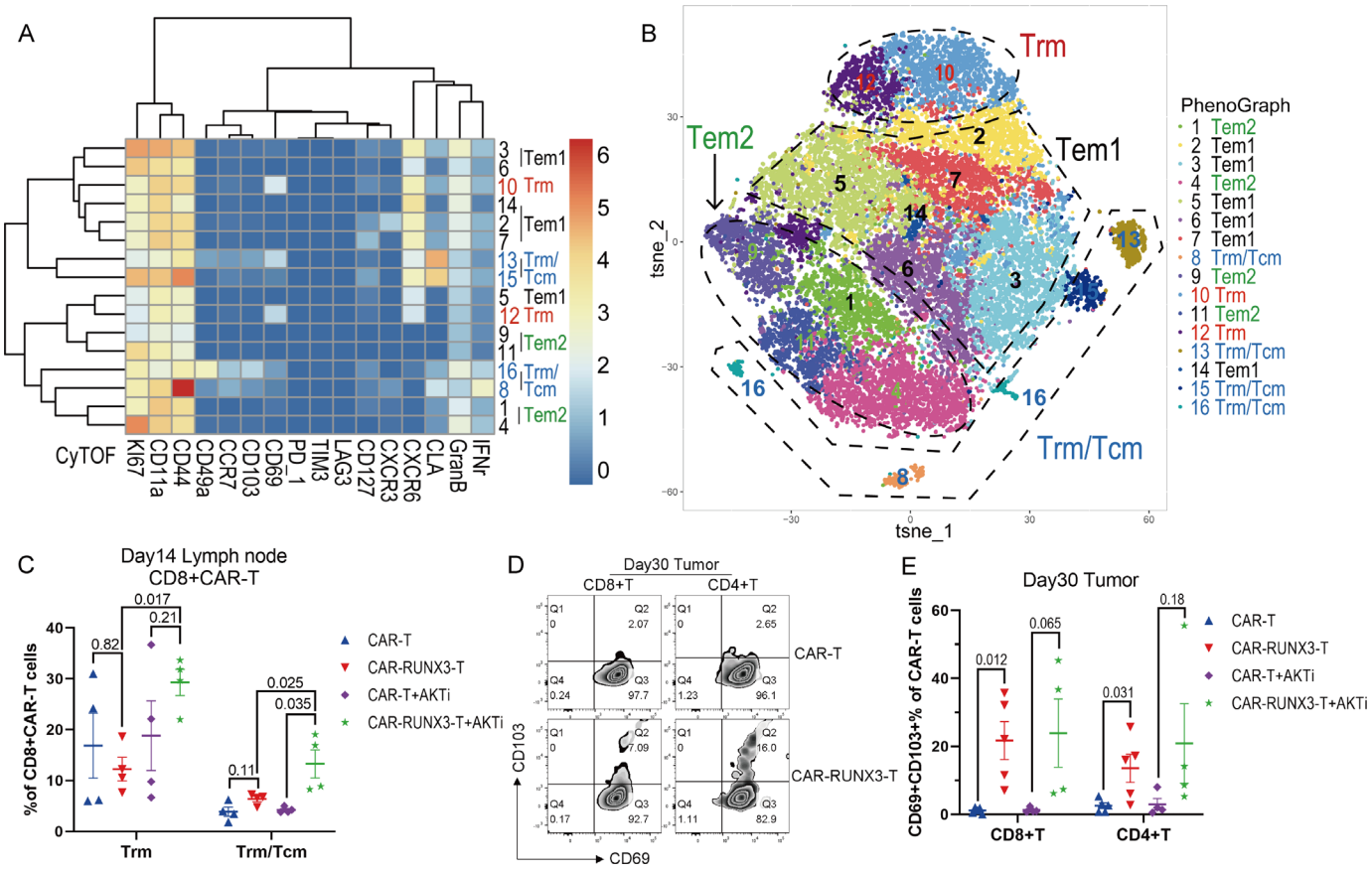

Figure 6 Runx3-overexpression cooperated with ex vivo AKTi to enrich T-cell population with both Trm and Tcm characteristics in vivo. (A) Heatmap of the expression of representative markers associated with Trm and Tcm phenotypes in different CD8+CAR T clusters. CAR-T cells were isolated from lymph nodes 14 days after CAR-T therapy. The expression of markers was quantified by CyTOF and clusters were identified by PhenoGraph method. (B) t-SNE map of CD8+CAR T cells expressing different markers detected by CyTOF. Clusters with similar markers were combined. (C) Percentages of Trm and Trm/Tcm cells in CD8+CAR T cells identified by CyTOF. CAR-T, normal CAR-T cells; CAR-RUNX3-T, Runx3-overexpressed CAR-T cells; AKTi, T cells were expended in 1 µM AKTi-1/2. (D) Representative flow cytometry plot and (G) percentages of CD69+CD103+ Trm cells in tumor-infiltrating CAR-T cells 30 days after adoptive therapy. A two-way analysis of variance was used for multiple comparisons in panels C and E, and p values were adjusted by Tukey method. P value<0.05 was considered statistically significant. AKT, protein kinase B; AKTi, AKT inhibition; CAR, chimeric antigen receptor; CyTOF, cytometry by time of flight; t-SNE, t-distributed stochastic neighbor embedding; RUNX3, RUNX family transcription factor 3; Tcms, central memory T cells ; Tems, effector memory T cells; Trms, tissue-resident memory T cells.

CCR7, while the Tem2 group had much lower expression of the Trm marker CXCR6 than the Tem1 group (figure 6B, online supplemental figure S7A). The combination of Runx3-OE and AKTi enriched the T-cell population with both Trm and Tcm characteristics (figure 6C). AKTi enriched T cells with Trm characteristics among Runx3-OE CAR-T cells (figure 6C), whereas Runx3-OE downregulated the Tem2 population and enriched the Tem1 population (online supplemental figure S7B). More specifically, Runx3-OE enriched clusters 2 and 3 (online supplemental figure S7C), which expressed CLA, CXCR6, and CXCR3 but did not express CD69 and CD103. Almost all the tumor-infiltrating CAR-T cells exhibited a CD69+ phenotype 30 days after adoptive therapy, whereas Runx3-OE promoted the formation of CD69+CD103+ Trm cells (figure 6D,E).

Thus, Runx3-OE cooperated with AKTi to enrich a T-cell population with both Trm and Tcm characteristics in vivo and promoted CAR-T-cell differentiation into the CD69+CD103+ Trm phenotype in tumors.

Ex vivo AKTi cooperated with Runx3-OE to promote CAR-T cell expansion and Runx3-OE further enhanced tumor-infiltrating CAR-T cell abundance in vivo

Then, we explored whether AKTi-generated CAR-T cells retained their strong expansion ability when combined with Runx3-OE in vivo. Thus, 10 million T cells with around 50% CAR-T cells were adoptively transferred into tumor-bearing nude mice (figure 7A). Seven days later, the weight of inguinal lymph nodes was larger in the AKTi groups than in the normal groups (figure 7B). We then analyzed the percentage of GFP+CAR T cells and Strep tag II+CAR-RUNX3-T cells within lymph nodes. AKTi significantly increased the percentage of T cells among CD45+ immune cells and did not decrease the percentage of CAR-T cells

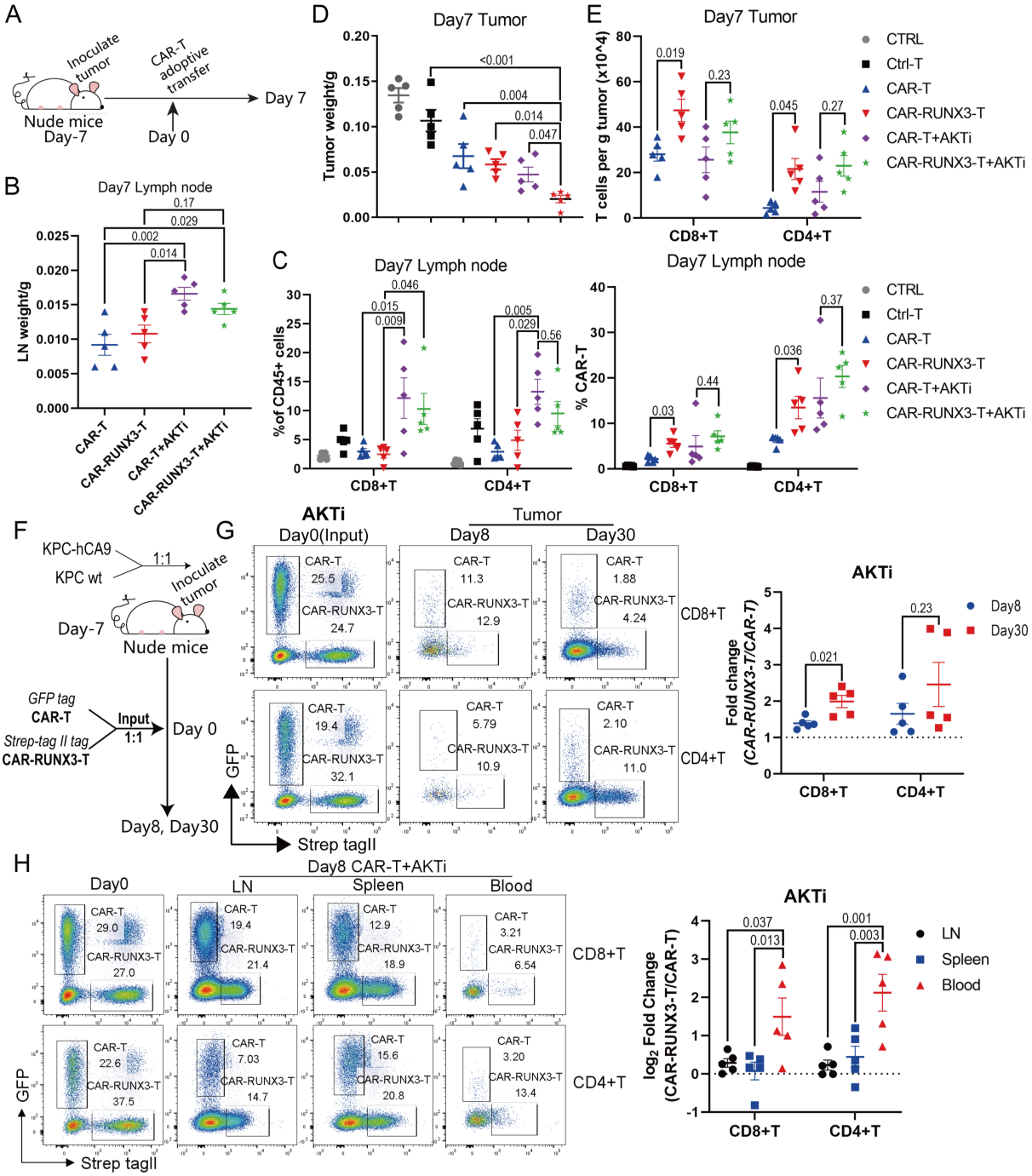

Figure 7 Ex vivo AKTi cooperated with Runx3-OE to promote CAR-T cell expansion and Runx3-OE further enhanced tumor-infiltrating CAR-T cell abundance in vivo. (A) Schematics of experiment; 10×10^6 T cells with 50% CAR-T cells were adoptively transferred into tumor-bearing nude mice. (B) Weight of inguinal lymph nodes 7 days after CAR-T therapy. CAR-T, normal CAR-T cells; CAR-RUNX3-T, Runx3-overexpressed CAR-T cells; AKTi, T cells were expended in 1 µM AKTi-1/2. (C) Percentages of T cells in CD45+ immune cells and percentages of CAR-T cells in T cells. Cells were isolated from inguinal lymph nodes 7 days after CAR-T therapy. (D) Tumor weight 7 days after CAR-T therapy. CTRL, no adoptive therapy; Ctrl-T, T cells without retroviral transduction. (E) Tumor infiltrating T-cell count per g tumor measured by flow cytometry. (F) Schematics of experiment; KPC and KPC-hCA9 cells (targeting cells) were mixed at a ratio of 1:1 and inoculated into the flank of nude mice. GFP+CAR T and Strep-tag II+CAR-RUNX3-T cells were mixed at a ratio of 1:1 and adoptively transferred into tumor-bearing nude mice. (G) Representative flow cytometry plot identifying tumor-infiltrating CAR-T and CAR-RUNX3-T cells. Fold change was calculated through dividing the ratio of CAR-RUNX3-T to CAR-T on day 8 or day 30 by that on day 0. (H) Representative flow cytometry plot identifying CAR-T and CAR-RUNX3-T cells in lymph nodes, spleens and blood. A one or two-way analysis of variance was used for multiple comparisons in panels B, C, D, E and H, and p values were adjusted by Tukey method. An unpaired two-tailed Student's t-test was used between two groups in panel G. P value<0.05 was considered statistically significant. AKT, protein kinase B; AKTi, AKT inhibition; CAR, chimeric antigen receptor; GFP, green fluorescent protein; hCA9, human carbonic anhydrase 9; LN, lymph node; RUNX3, RUNX family transcription factor 3; RUNX3-OE, RUNX3-overexpression.

among T cells (figure 7C, online supplemental figure S8A). Thus, AKTi always promoted CAR-T cell expansion in vivo, regardless of *Runx3*-OE.

Next, we confirmed whether Runx3-OE improved CAR-T cell tumor residency. Tumors treated with AKTi-generated CAR-RUNX3-T cells had the lowest weights and volumes (figure 7D, online supplemental figure figure S8B), which was consistent with our previous results (figure 5). We then counted tumor-infiltrating T cells (online supplemental figure S8C). There were significantly more tumor-infiltrating T cells per gram of tumor in the CAR-RUNX3-T group than in the CAR-T group, while no statistical significance was noted between the CAR-RUNX3-T+AKTi group and the CAR-T+AKTi group (figure 7E).

Importantly, it was difficult to accurately measure the counts of tumor-infiltrating CAR-T cells in disappearing tumors in the CAR-RUNX3-T+AKTi group. Thus, we mixed KPC and KPC-hCA9 cells at a ratio of 1:1 and inoculated them into the flank of nude mice to prevent the disappearance of tumors (figure 7F). Next, we mixed GFP+CAR T and Strep tag II+CAR-RUNX3-T cells at a ratio of 1:1 and adoptively transferred them into tumor-bearing nude mice (figure 7F). The ratio of CAR-RUNX3-T and CAR-T was not strictly 1:1 on day 0; therefore, the evaluation index of fold change was introduced, which was calculated by dividing the ratio of CAR-RUNX3-T to CAR-T on day 8 or day 30 by that on day 0. The fold change was greater than 1 on day 8 and day 30 (figure 7G, online supplemental figure S8D), indicating that Runx3-OE enhanced tumor-infiltrating CAR-T cell abundance.

Moreover, the average $\log_2$fold change was greater than 0 in lymph nodes and blood on day 8 (figure 7H), indicating that Runx3-OE promoted CAR-T cell expansion, which was consistent with our previous results (figure 3E–H and figure 7C). The $\log_2$fold change was greater in blood than in lymph nodes (figure 7H, online supplemental figure S8E), suggesting that Runx3-OE promoted CAR-T cell transfer into blood from lymph nodes. The transcriptomic analysis had shown that Runx3-OE upregulated the expression of *Ccr2* and *Ccr5*, as well as KEGG pathways involved in tumor-infiltration (figure 3A, figure 7H and online supplemental figure S9H). We confirmed the upregulation of CCR2 by Runx3-OE on ex vivo CAR-T cells using flow cytometry (online supplemental figure S8F,G).

Thus, AKTi cooperated with Runx3-OE to promote CAR-T cell expansion and Runx3-OE further enhanced tumor-infiltrating CAR-T cell abundance in vivo.

Runx3-OE cooperated with AKTi to enhance the persistence, cytotoxic potential, and antitumor activity of human CAR-T cells

Next, we sought to prove that Runx3-OE cooperated with AKTi to generate CAR-T cells with both tissue-resident and central-memory characteristics in human T cells in addition to murine T cells. Therefore, we created new plasmids for the human version that expressed CAR and Runx3 together or the CAR alone based on a lentiviral backbone (online supplemental figure S9A). Then, we performed human peripheral blood mononuclear cell isolation, T-cell activation, lentiviral transduction, and expanded CAR-T cells in the presence of 1 µM AKTi-1/2 or vehicle (online supplemental figure S9B). Runx3-OE cooperated with AKTi to enhance the percentage of CAR-T cells among T cells (online supplemental figure S9C,D), suggesting enhanced persistence. AKTi increased the percentage of Tcm among CAR-T cells, while Runx3-OE promoted the percentage of Te among CAR-T cells (online supplemental figure S9E). Runx3-OE upregulated the expression of GzmB and promoted CAR-T cells to exhibit CD69+GzmB+ Trm characteristics after co-incubation with target cells (online supplemental figure S9F). Runx3-OE promoted the cytolytic ability of CAR-T cells, especially in CD4+T cells (online supplemental figure S9G). Meanwhile, Runx3-OE cooperated with AKTi to enhance the antitumor activity of CAR-T cells in human PDAC cell line-derived xenograft mouse models (online supplemental figure S9H). Thus, AKTi promoted the central-memory phenotype while Runx3-OE promoted tissue-resident characteristics in human CAR-T cells, and they cooperated to enhance the persistence, cytotoxic potential, and antitumor activity of human CAR-T cells.

DISCUSSION

Herein, we demonstrated that Runx3-OE cooperated with AKTi to generate CAR-T cells with better persistence, tumor-residency, and antitumor ability. AKTi promoted the CAR-T cell Tcm phenotype and enhanced persistence, while Runx3-OE promoted the CAR-T cell Trm phenotype to further enhance persistence, effector function, and tumor-residency (online supplemental figure S10A,B). Moreover, Runx3-OE cooperated with AKTi to inhibit CD8+CAR T-cell terminal differentiation induced by tonic signaling.

Limited T-cell survival before reaching tumor sites is the first roadblock for CAR-T therapy.[3 4] To overcome this problem, we added AKTi-1/2 to the conventional T-cell manufacturing process and generated CD62L+Tcm like CAR-T cells.[12 13 28] We confirmed that 1 µM AKTi-1/2 was optimal for our intended purpose and AKTi-generated CAR-T cells showed enhanced persistence and antitumor activity in vivo, consistent with previous studies.[12 13] Urak *et al* explained that AKT inhibition did not dampen human CAR-T cell mediated cytotoxicity,[12] we found that AKTi-1/2 at 1 µM did not impair human CAR-T cell cytotoxicity, but impaired the cytotoxic potential of mCAR-T cells. We hypothesized that mCAR-T cells responded more strongly to AKTi than human CAR-T cells. Indeed, herein, 1 µM AKTi-1/2 generated mCAR-T cells with a 90% Tcm population, but

generated human CAR-T cells with a 40% Tcm population. The optimal concentration of AKTi-1/2 might vary between different species.

Next, we sought to enhance the cytotoxic potential of AKTi-generated Tcm-like mCAR-T cells while maintaining their increased persistence. Trms represent a heterogeneous T-cell population that function as both effector and memory T cells, and express residence gene signatures, unlike Tems.[17] These features allow them to traffic to, reside in, and potentially patrol peripheral tissues, thereby exerting an efficient long-term immune-protective role.[17] RUNX3 programed CD8+T cell residency in non-lymphoid tissues and tumors[18]; ectopic expression of Runx3 in CD4+T cells drove a CD8+T like tissue residency program, which was absent in natural CD4+T cells[29]; therefore, we overexpressed *Runx3* in the AKTi-generated CAR-T cells and successfully generated CAR-T cells with both Tcm and Trm characteristics.

Trm cells have properties of effector cells, thus Runx3-OE in CD4+T cells enhanced the expression of GzmB and IFN-γ, as well as their cytotoxic potential. However, we noticed that Runx3-OE downregulated the expression of effector molecules (GzmB, perforin and IFN-γ) in CD8+CAR T cells, inconsistent to Milner *et al*'s results.[18] It was because our CAR elicited high ligand independent constitutive tonic signaling, which is associated with accelerated T-cell terminal differentiation.[30] RUNX3 drives the differentiation of nascent cytotoxic T lymphocytes (CTLs) and also represses terminal differentiation to ensure the development of long-lived memory CTLs.[31] Thus, Runx3-OE showed its function of inhibiting CD8+CAR T-cell terminal differentiation induced by tonic signaling.

Milner *et al* also found Runx3-OE promoted the antitumor activity of P14 T cells[18]; however, herein, Runx3-OE alone did not promote the antitumor activity of CAR-T cells. We found only a minority of our Runx3-OE CAR-T cells exhibited a Tcm phenotype at the late period of expansion, indicating poor ability of expansion and persistence. Perhaps, the insufficient proportion of the Tcm population limited the effect of Runx3-OE. It was a pity that we did not know the proportion of various T-cell subsets among P14 T cells. Nevertheless, our new CAR-T cells with both Tcm and Trm characteristics exhibited enhanced persistence, effector function, tumor residency and antitumor activity. Trm cells seem to resemble effector cells because of their expression of PD-1, IFN-γ, perforin, and GzmB,[32 33] and share properties with stem cells, being long-lived and not terminally differentiated.[32] Thus, our AKTi-generated *Runx3*-OE CAR-T cells with Trm characteristics responded well to PD-1 blockade, while AKTi-generated CAR-T cells did not.

Finally, we confirmed that Runx3-OE combined with AKTi enhanced the persistence, cytotoxic potential, and antitumor activity of human CAR-T cells. AKTi-1/2 at 1 μM did not inhibit AKT phosphorylation optimally (data not shown) in human CAR-T cells; therefore, Runx3-OE and AKTi had dynamic effects on human T-cell phenotypes: While AKTi increased the percentage of the Tcm population, Runx3-OE promoted CD69+GzmB+ Trm characteristics. Thus, our strategy of combining Runx3-OE with AKTi also worked well in human T cells. AKTi-1/2 at 1 μM might not be optimal for human CAR-T cells and the optimal concentration of AKTi-1/2 might also vary among various T-cell subsets as starting populations[12]; therefore, further titration of the AKT inhibitor for human T cells is needed. 4-1BB co-stimulation was reported to ameliorate T-cell exhaustion induced by tonic signaling.[27] Therefore, we constructed third generation CAR-T cells based on intracellular CD28 and 4-1BB domains instead of second generation CAR-T cells based on CD28 domains, because our CAR-T cells had high levels of tonic signaling. We did not confirm the antitumor activity of the AKTi-generated Runx3-OE CAR-T cells in immunocompetent mice because the overexpression of human proteins in the KPC cell line limits their growth in immunocompetent mice.

In summary, *Runx3*-OE cooperated with ex vivo AKTi to generate CAR-T cells with better persistence, cytotoxic potential, tumor-residency, and antitumor activity. CAR-T cells with both tissue-resident and central memory characteristics are better equipped to overcome the roadblocks for treating solid tumors. Attempts should be made to improve CAR-T therapy by combining the advantages of different phenotypes while compensating for their disadvantages.

Author affiliations
[1]Zhejiang Provincial Key Laboratory of Pancreatic Disease, Zhejiang University School of Medicine First Affiliated Hospital, Hangzhou, Zhejiang, China
[2]Department of Hepatobiliary and Pancreatic Surgery, Zhejiang University School of Medicine First Affiliated Hospital, Hangzhou, Zhejiang, China
[3]Zhejiang Provincial Innovation Center for the Study of Pancreatic Diseases, Zhejiang University, Hangzhou, Zhejiang, China
[4]Cancer Center, Zhejiang University, Hangzhou, Zhejiang, China

Contributors Study concept and design: JT, JpS, QZ, XB, TL. Acquisition of data: JT, YJ, XW, JZ, JW, JyS. Data analysis: JT, JpS. Obtained funding: JpS, XB, TL. Study supervision: JT, JpS, QZ, XB, TL. Drafting of manuscript: JT. Critical revision of manuscript: JpS, TL. The guarantor: TL.

Competing interests No, there are no competing interests.

Patient consent for publication Not applicable.

Ethics approval Not applicable.

Provenance and peer review Not commissioned; externally peer reviewed.

Data availability statement Data are available upon reasonable request. The data analyzed in this study were obtained from Gene Expression Omnibus (GEO) at GSE107395. The data generated in this study are available upon request from the corresponding author Prof. Tingbo Liang (liangtingbo@zju.edu.cn).

Supplemental material This content has been supplied by the author(s). It has not been vetted by BMJ Publishing Group Limited (BMJ) and may not have been peer-reviewed. Any opinions or recommendations discussed are solely those of the author(s) and are not endorsed by BMJ. BMJ disclaims all liability and responsibility arising from any reliance placed on the content. Where the content includes any translated material, BMJ does not warrant the accuracy and reliability of the translations (including but not limited to local regulations, clinical guidelines, terminology, drug names and drug dosages), and is not responsible for any error and/or omissions arising from translation and adaptation or otherwise.

Open access This is an open access article distributed in accordance with the Creative Commons Attribution Non Commercial (CC BY-NC 4.0) license, which permits others to distribute, remix, adapt, build upon this work non-commercially, and license their derivative works on different terms, provided the original work is properly cited, appropriate credit is given, any changes made indicated, and the use is non-commercial. See http://creativecommons.org/licenses/by-nc/4.0/.

ORCID iDs
Xueli Bai http://orcid.org/0000-0002-2934-0880
Tingbo Liang http://orcid.org/0000-0003-3262-2587

REFERENCES

1 Larson RC, Maus MV. Recent advances and discoveries in the mechanisms and functions of CAR T cells. *Nat Rev Cancer* 2021;21:145–61.
2 Wagner J, Wickman E, DeRenzo C, *et al*. Car T cell therapy for solid tumors: bright future or dark reality? *Mol Ther* 2020;28:2320–39.
3 Rafiq S, Hackett CS, Brentjens RJ. Engineering strategies to overcome the current roadblocks in car T cell therapy. *Nat Rev Clin Oncol* 2020;17:147–67.
4 Chan JD, Lai J, Slaney CY, *et al*. Cellular networks controlling T cell persistence in adoptive cell therapy. *Nat Rev Immunol* 2021;21:769–84.
5 van der Woude LL, Gorris MAJ, Halilovic A, *et al*. Migrating into the tumor: a roadmap for T cells. *Trends Cancer* 2017;3:797–808.
6 Lanitis E, Dangaj D, Irving M, *et al*. Mechanisms regulating T-cell infiltration and activity in solid tumors. *Ann Oncol* 2017;28(suppl_12):xii18–32.
7 Hou AJ, Chen LC, Chen YY. Navigating CAR-T cells through the solid-tumour microenvironment. *Nat Rev Drug Discov* 2021;20:531–50.
8 Rodriguez-Garcia A, Palazon A, Noguera-Ortega E, *et al*. Car-T cells hit the tumor microenvironment: strategies to overcome tumor escape. *Front Immunol* 2020;11:1109.
9 Fraietta JA, Nobles CL, Sammons MA, *et al*. Disruption of TET2 promotes the therapeutic efficacy of CD19-targeted T cells. *Nature* 2018;558:307–12.
10 Giuffrida L, Sek K, Henderson MA, *et al*. Il-15 preconditioning augments CAR T cell responses to checkpoint blockade for improved treatment of solid tumors. *Mol Ther* 2020;28:2379–93.
11 Gong W, Hoffmann J-M, Stock S, *et al*. Comparison of IL-2 vs IL-7/IL-15 for the generation of NY-ESO-1-specific T cells. *Cancer Immunol Immunother* 2019;68:1195–209.
12 Urak R, Walter M, Lim L, *et al*. Ex vivo akt inhibition promotes the generation of potent CD19CAR T cells for adoptive immunotherapy. *J Immunother Cancer* 2017;5:26.
13 Klebanoff CA, Crompton JG, Leonardi AJ, *et al*. Inhibition of akt signaling uncouples T cell differentiation from expansion for receptor-engineered adoptive immunotherapy. *JCI Insight* 2017;2:23.
14 Abu Eid R, Ahmad S, Lin Y, *et al*. Enhanced therapeutic efficacy and memory of tumor-specific CD8 T cells by ex vivo PI3K-δ inhibition. *Cancer Res* 2017;77:4135–45.
15 Muralidharan S, Hanley PJ, Liu E, *et al*. Activation of Wnt signaling arrests effector differentiation in human peripheral and cord blood-derived T lymphocytes. *J Immunol* 2011;187:5221–32.
16 Tantalo DG, Oliver AJ, von Scheidt B, *et al*. Understanding T cell phenotype for the design of effective chimeric antigen receptor T cell therapies. *J Immunother Cancer* 2021;9:e002555.
17 Okła K, Farber DL, Zou W. Tissue-Resident memory T cells in tumor immunity and immunotherapy. *J Exp Med* 2021;218:e20201605.
18 Milner JJ, Toma C, Yu B, *et al*. Runx3 programs CD8+ T cell residency in non-lymphoid tissues and tumours. *Nature* 2017;552:253–7.
19 Cui J, Zhang Q, Song Q, *et al*. Targeting hypoxia downstream signaling protein, CAIX, for CAR T-cell therapy against glioblastoma. *Neuro Oncol* 2019;21:1436–46.
20 Liu L, Sommermeyer D, Cabanov A, *et al*. Inclusion of strep-tag II in design of antigen receptors for T-cell immunotherapy. *Nat Biotechnol* 2016;34:430–4.
21 Kurachi M, Kurachi J, Chen Z, *et al*. Optimized retroviral transduction of mouse T cells for in vivo assessment of gene function. *Nat Protoc* 2017;12:1980–98.
22 Pear W. Transient transfection methods for preparation of high-titer retroviral supernatants. *Curr Protoc Mol Biol* 2001;Chapter 9:Unit9.
23 Sheng J, Zhang J, Wang L, *et al*. Topological analysis of hepatocellular carcinoma tumour microenvironment based on imaging mass cytometry reveals cellular neighbourhood regulated reversely by macrophages with different ontogeny. *Gut* 2022;71:1176–91.
24 Macintyre AN, Finlay D, Preston G, *et al*. Protein kinase B controls transcriptional programs that direct cytotoxic T cell fate but is dispensable for T cell metabolism. *Immunity* 2011;34:224–36.
25 Mackay LK, Rahimpour A, Ma JZ, *et al*. The developmental pathway for CD103 (+) CD8+ tissue-resident memory T cells of skin. *Nat Immunol* 2013;14:1294–301.
26 Szabo PA, Miron M, Farber DL. Location, location, location: tissue resident memory T cells in mice and humans. *Sci Immunol* 2019;4:34.
27 Long AH, Haso WM, Shern JF, *et al*. 4-1Bb costimulation ameliorates T cell exhaustion induced by tonic signaling of chimeric antigen receptors. *Nat Med* 2015;21:581–90.
28 Crompton JG, Sukumar M, Roychoudhuri R, *et al*. Akt inhibition enhances expansion of potent tumor-specific lymphocytes with memory cell characteristics. *Cancer Res* 2015;75:296–305.
29 Fonseca R, Burn TN, Gandolfo LC, *et al*. Runx3 drives a CD8+ T cell tissue residency program that is absent in CD4+ T cells. *Nat Immunol* 2022;23:1236–45.
30 Calderon H, Mamonkin M, Guedan S. Analysis of CAR-mediated tonic signaling. *Methods Mol Biol* 2020;2086:223–36.
31 Wang D, Diao H, Getzler AJ, *et al*. The transcription factor RUNX3 establishes chromatin accessibility of cis-regulatory landscapes that drive memory cytotoxic T lymphocyte formation. *Immunity* 2018;48:659–74.
32 Milner JJ, Goldrath AW. Transcriptional programming of tissue-resident memory CD8+ T cells. *Current Opinion in Immunology* 2018;51:162–9.
33 Ganesan A-P, Clarke J, Wood O, *et al*. Tissue-Resident memory features are linked to the magnitude of cytotoxic T cell responses in human lung cancer. *Nat Immunol* 2017;18:940–50.